ACS Energy LETTERS

Cite This: ACS Energy Lett. 2018, 3, 940−945

LETTER

Surface Evolution of PtCu Alloy Shell over Pd Nanocrystals Leads to Superior Hydrogen Evolution and Oxygen Reduction Reactions

Mingjun Bao,[†,⊥] Ibrahim Saana Amiinu,[†,⊥] Tao Peng,[‡] Wenqiang Li,[†] Shaojun Liu,[†] Zhe Wang,[†] Zonghua Pu,[†] Daping He,*[,†,§] Yuli Xiong,*[,∥] and Shichun Mu*[,†]

[†]State Key Laboratory of Advanced Technology for Materials Synthesis and Processing, Wuhan University of Technology, Wuhan 430070, China

[‡]Department of Civil and Environmental Engineering, University of Windsor, 401 Sunset Avenue, Windsor, Ontario N9B 3P4, Canada

[§]Hubei Engineering Research Center of RF-Microwave Technology and Application, Wuhan University of Technology, Wuhan 430070, China

[∥]Michael Grätzel Center for Mesoscopic Solar Cells (MGC), Wuhan National Laboratory for Optoelectronics, School of Optical and Electronic Information, Huazhong University of Science and Technology, Wuhan 430074, China

Supporting Information

ABSTRACT: **Pt-based electrocatalysts are by far the most effective for the hydrogen evolution reaction (HER) and oxygen reduction reaction (ORR), but they still suffer from high cost and insufficient overall performance. Improving Pt utilization via alloying or by forming core@shell structures is important for enhancing Pt activity and overall electrocatalytic performance. Herein, we report a simple seed-mediated method for synthesizing a dodecahedral PtCu alloy atomic shell on Pd nanocrystals. Significantly, such a Pd@PtCu nanocomposite with unique core@alloy-shell structure achieves a 25-fold and 6-fold enhancement of mass activity for HER and ORR, respectively, compared with the commercial Pt/C catalyst in acid media. Moreover, the unique Pd@PtCu catalyst shows only 1.0 mV increase in overpotential at 10 mA cm^{-2} after 10 000 cycles for HER and almost no activity decay after 5 000 cycles for ORR, indicating the high endurance of Pd@PtCu in the electrochemical environment.**

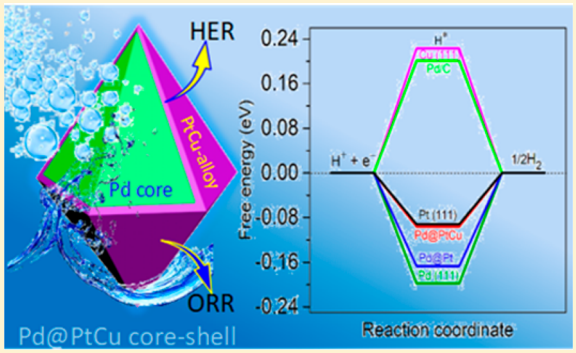

Currently, both the electrocatalytic hydrogen evolution reaction (HER) for hydrogen generation via water splitting and the oxygen reduction reaction (ORR) at the cathode for polymer electrolyte membrane fuel cells (PEMFCs) are highly important catalytic processes for clean and renewable energy conversion devices.[1−3] Although tremendous efforts have been taken to find alternative catalyst materials, hitherto, Pt-based electrocatalysts are still the best commercial catalyst for both electrochemical reactions. However, the high cost, low Pt utilization, and insufficient durability of such Pt-based electrocatalysts remain as the major bottlenecks for their commercialization and widespread applications.[4−6] Therefore, the development of renewable electrocatalysts with decreasing Pt usage and high performance for HER and ORR is urgently desired to achieve cost-effective energy conversion.

The core@shell nanostructure with ultrathin Pt shell has been widely reported as a suitable strategy for decreasing the content of scarce Pt, as well as boosting the electrocatalytic efficiency. In particular, when Pt is deposited on a substrate metal to form a Pt shell structure, lattice expansion or compression may occur because of the lattice mismatch between Pt and the substrate. For instance, a tensile strain occurs when Pt is deposited on Au substrates, while a compressive strain is induced when Pt is deposited on Ru.[7] The generated surface strains can affect the surface charge state and consequently change the binding energy of adsorbates on Pt, which is important for enhancing the electrocatalytic activity of Pt catalysts toward both ORR and HER.[8−11] Our previous work has successfully prepared icosahedral Pd@Pt core−shell and ultrathin Pt-enriched nanocage crystals with improved

Received: February 27, 2018
Accepted: March 16, 2018

DOI: 10.1021/acsenergylett.8b00330
ACS Energy Lett. 2018, 3, 940−945

ORR activity via the deposition of well-controlled Pt layers on Pd icosahedral seeds.[12] Xiong et al. reported that the surface polarization of Pt on Pd can improve the HER performance.[13] On the other side, alloying Pt with another less expensive metal is another effective way to reduce Pt usage. Substantial works have been done on Pt−M (usually transition metals) alloys such as Pt−nickel (Pt−Ni), Pt−cobalt (Pt−Co), Pt−iron (Pt−Fe), and Pt−copper (Pt−Cu), with well-controlled structure and morphology, which exhibit enhanced activity and durability as electrocatalysts for ORR and HER.[14−19] Considering the critical role of the Pt shell in the core@shell structure catalysts and the need to further decrease the Pt amount, developing a Pt−M alloy shell instead of a single-component shell for activating electrocatalysis may have more advantages, although this is still a big challenge.

In this work, we designed and synthesized a dodecahedral Pd@PtCu nanocrystal with a core@alloy-shell structure by a simple seed-mediated approach. Owing to the synergistic effect between Pt and Cu, as well as the high utilization efficiency of Pt in the PtCu alloy shell, the dodecahedral Pd@PtCu core−shell nanocrystal shows both superior HER and ORR catalytic activity and stability in comparison with commercial Pt/C. This work not only reveals the effect of the Pd substrate but also highlights the significant effect of the PtCu alloy shell on both HER and ORR catalytic activity.

The synthesis routes of Pd@PtCu and Pd@Pt nanocrystals are illustrated in Figure 1. Generally, the synthesis of Pd@PtCu

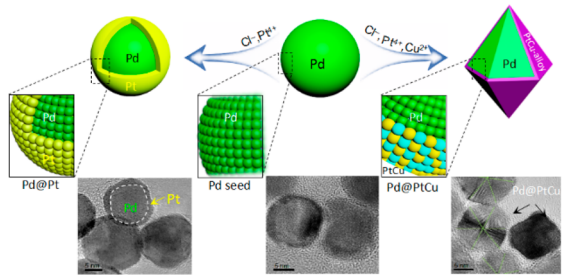

Figure 1. Schematic illustration of the preparation of Pd@Pt and Pd@PtCu core−shell nanocrystals and corresponding TEM images.

and Pd@Pt involves the formation of Pd seeds and PtCu or Pt coating on the Pd to form a nanoshell (see details in the Supporting Information). In the synthesis process of Pd@PtCu nanoparticles, Cu^{2+} ions are more likely adsorbed at the surface of the Pd core, then the PtCu alloy will most likely grow along the {111} crystal surface and finally form a polyhedral structure instead of a sphere, so the morphology of Pd@PtCu tends to form a dodecahedral structure in the presence of Cu^{2+} and Cl^- because of the selective adsorption processes.[20−24] Figure S1 is the high-resolution transmission electron microscopy (HRTEM) image of Pd seeds which were used as the seed for Pt and Cu deposition in the formation of Pt@Pd and Pd@PtCu core−shell structures. For Pd@Pt nanoparticles (Figure S2), the lattice of Pt is very close to that of Pd, so the growth of the Pt shell follows the epitaxial growth of the Pd core.

From Figure 2a−c, it can be observed that Pd@PtCu nanoparticles have a very uniform particle size distribution (around 15 nm, Figure S3) with a universal dodecahedral structure. Panels d and e of Figure 2 are the top and frontal views, respectively, of the atomic resolution HRTEM images of a Pd@PtCu nanoparticle, with corresponding models displayed in the insets for comparison, which show the characteristic

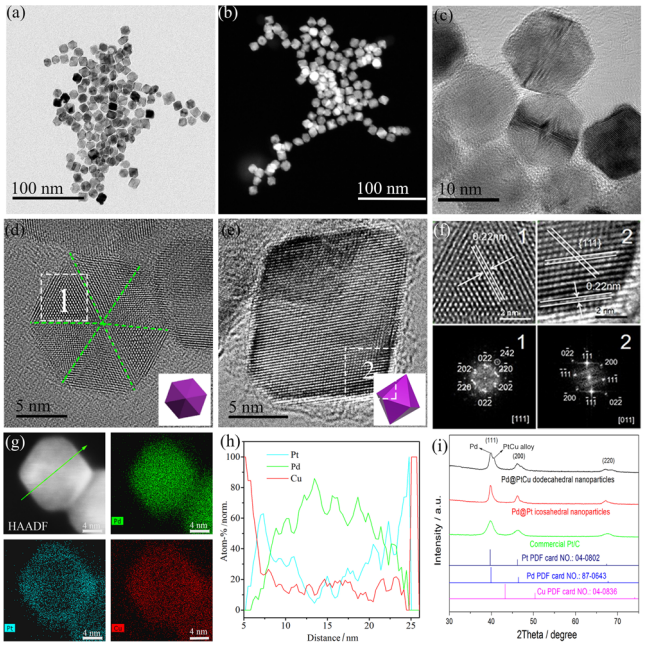

Figure 2. (a) Low-magnification aberration-corrected (AC) TEM image and (b) HAADF-STEM image of Pd@PtCu core−shell dodecahedral nanoparticles. (c) High magnification AC-TEM image of Pd@PtCu core−shell dodecahedral nanocrystals. (d) Top view and (e) frontal view of the aberration-corrected HRTEM images of one single Pd@PtCu core−shell dodecahedral nanocrystal. The insets of panels d and e are the respective top view and front view models of Pd@PtCu core−shell dodecahedral nanoparticle. (f) Selected area magnification images and FFT of 1 and 2. (g) HAADF-STEM image of Pd@PtCu core−shell dodecahedral nanoparticle and EDX mapping (green, Pd; aqua, Pt; and red, Cu). (h) EDS line scan of Pd, Pt, and Cu along the arrowed line in panel g recorded from Pd@PtCu core−shell nanocrystal. (i) XRD spectra of Pd@Pt core−shell nanocrystal, Pd@PtCu core−shell nanocrystal, and Pt/C [standard PDF card no. Pt (04-0802), Pd (87-0643), and Cu (04-0836)].

lattice fringe of the dodecahedral. Figure 2f shows the magnified TEM images and the corresponding fast Fourier transforms (FFTs) of the regions marked by square dotted lines in Figure 2d,e. The lattice spacing of 0.22 nm can be indexed to {111} planes of the "PtCu alloy shell". Because of the atomic contrast (Z contrast), Pt signals are darker than Pd signals; therefore, it can be clearly observed that a few layers of PtCu alloy epitaxially grew on the Pd seed surface to form the PtCu alloy shell microstructure. The FFT in Figure 2f shows the [111] and [011] diffractograms for the selected area marked as 1 and 2, respectively. From the energy-dispersive X-ray (EDX) mapping (Figure 2g), the signals of Pd and Pt occur on the core and shell, respectively, while Cu signals exist on both core and shell, which is mainly because of the Kirkendall effect.[25] The occurrence of this in situ replacement and the formation of the core−shell structure were further proven by EDS line scanning (Figure 2h). As shown in Figure 2i, there are two distinct sets of diffraction peaks for Pd@PtCu that could be ascribed to the Pd and PtCu alloy, respectively, indicating the existence of PtCu alloy and the formation of Pd@PtCu core−shell structure. As determined by inductively coupled plasma−optical emission spectroscopy measurements, the atomic percentage of Pt, Pd, and Cu in the Pd@PtCu core−shell nanoparticles are 12.5, 82.6, and 4.9 at %, respectively, which also coincides with the result of EDX measurements (Figure

DOI: 10.1021/acsenergylett.8b00330
ACS Energy Lett. 2018, 3, 940−945

S4). Furthermore, the surface chemical state and detailed elemental composition of Pd@PtCu core−shell nanoparticles were investigated by XPS, which reveals that the surface of Pd@PtCu nanoparticles is mainly composed of Pt, Pd, and Cu (Figure S5a). As shown in Figure S5b, we can see that the binding energies of Pt $4f_{7/2}$ and Pt $4f_{5/2}$ peaks are 71.1 and 74.5 eV, respectively, which are very close to the Pt (0) (71.0 and 74.4 eV).[26] The Pd $3d_{5/2}$ and Pd $3d_{3/2}$ peaks (Figure S5c) are located at 335.2 and 340.5 eV, respectively, also near the zero valence of Pd (335.0 and 340.3 eV).[26] By analyzing the XPS spectra of Pt 4f and Pd 3d, we can find that Pt and Pd mainly exist in a zero valence state, which is beneficial for catalytic performance as Pt (0) is much more electroactive than Pt (+2) and Pt (+4). In Figure S5d, the peaks at 932.0 and 951.8 eV correspond to the binding energy of Cu (0) $2p_{3/2}$ and Cu (0) $2p_{1/2}$, while the peaks at 934.0 and 953.1 eV are associated with the Cu (+2) $2p_{3/2}$ and Cu (+2) $2p_{1/2}$, respectively, owing to the unavoidable mild surface oxidation upon exposure to air.[27] Above all, the Cu atoms are more reactive than Pt and Pd, which is beneficial for protecting Pt and Pd elements from oxidization.

The HER measurements for Pd@PtCu/C, Pd@Pt/C, commercial Pt/C, and commercial Pd/C catalysts are summarized in Figure 3. All of the catalysts coated on the glassy carbon electrodes had the same Pt loading of 15 μg cm^{-2}. Figure 3a shows the HER polarization curves with *iR*-correction in 0.5 M H_2SO_4 at room temperature by linear sweep voltammetry at a scan rate of 5 mV/s. From the curves, we can see that Pd@PtCu/C displays the smallest overpotential among these four catalysts. At a current density of 10 mA cm^{-2}, the overpotential of Pd@PtCu/C is only 19 mV versus the reversible hydrogen electrode (RHE) which is 5 and 12 mV smaller than that of the Pd@Pt/C counterpart and commercial Pt/C catalysts, respectively. To investigate the inherent properties of the catalyst material and the rate-determining step of the overall hydrogen evolution process, the Tafel slope was obtained from the HER polarization curves. As shown in Figure 3b, the calculated Tafel slope of Pd@PtCu is 26.2 mV/decade, which is much smaller than that of Pd@Pt (30.1 mV/decade), Pt/C (30.4 mV/decade), and Pd/C (110.5 mV/decade) catalysts, further evidencing that Pd@PtCu/C has outstanding HER electrocatalytic properties. The mass activity at an overpotential of 25 mV for the different electrocatalysts are presented in Figure 3c. It can be seen that Pd@PtCu/C has the largest mass activity of 6.6 A mg_{Pt}^{-1}, which is about ∼9 and ∼25 times higher than that of Pd@Pt/C (0.74 A mg_{Pt}^{-1}) and commercial Pt/C (0.26 A mg_{Pt}^{-1}). The accelerated degradation test (ADT) in acidic medium was used to probe the stability of the Pd@PtCu/C catalyst (Figure 3d). After 10 000 cycles, the Pd@PtCu/C increases by only ∼1.0 mV in overpotential at a current density of 10 mA cm^{-2}, whereas Pt/C shows an increase of ∼24 mV.

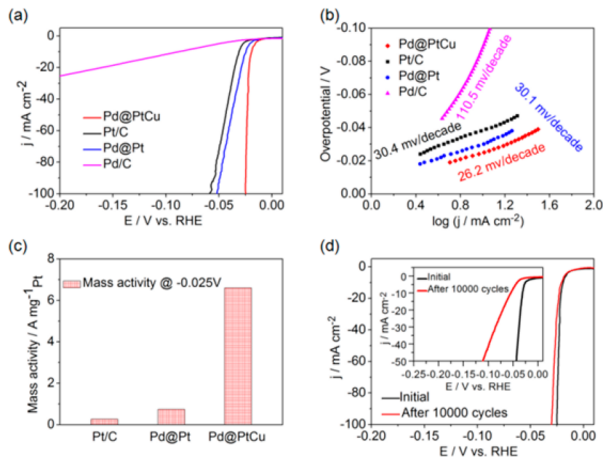

Figure 3. HER electrocatalytic properties: (a) HER polarization curves of Pd@PtCu/C, Pd@Pt/C, Pd/C and Pt/C, acquired by linear sweep voltammetry with a scan rate of 5 mV/s in 0.5 M H_2SO_4 at room temperature. (b) Tafel plots of catalysts obtained from the polarization curves in panel a. (c) Mass activity at −0.025 V versus RHE for Pd@PtCu/C, Pd@Pt/C, and Pt/C. (d) Stability of Pd@PtCu/C versus commercial Pt/C catalyst (inset). The polarization curves were recorded before and after 10 000 CV sweeps between +0.05 and −0.15 V in 0.5 M H_2SO_4 at room temperature at a scan rate of 5 mV/s.

As shown in Figure S6a, the HER activity and stability in alkaline media were also probed. We can see that Pd@PtCu/C also exhibits the best HER activity in alkaline media among the four catalysts. At the current density of 10 mA cm^{-2}, the overpotential of Pd@PtCu/C is just 60 mV vs RHE, which is ∼10, ∼19, and ∼42 mV smaller than that of Pd@Pt/C (70 mV), Pt/C (79 mV), and Pd/C (102 mV), respectively. Such a high HER activity is also superior to that of recently reported Pt-based catalysts including Pt−Ni,[28] Pt−Ag,[29] and Pt@NHPCP,[30] as well as other noble or highly active transition-metal-based HER catalysts (Table S1). Figure S6b presents the durability test of Pd@PtCu/C and commercial Pt/C catalyst (inset). Interestingly, after 10 000 cycles of the ADT, commercial Pt/C shows an increase of overpotential by about 17 mV at the current density of 10 mA cm^{-2}, whereas the Pd@PtCu/C overpotential rather decreases by ∼7 mV in alkaline electrolyte. This anomalous increase in HER activity of Pd@PtCu/C after the ADT can be assigned to gradual etching by selective attack and erosion of reactive Cu and Pd atoms, leading to further exposure of more active edges of Pt for HER kinetic activity.

Density functional theory (DFT) was employed to gain more in-depth understanding of the high HER activity of the electrocatalysts (see details in the Supporting Information). The Gibbs free energy (ΔG_{H^*}) for the chemisorption of hydrogen is well-known to be strongly correlated to the catalytic HER activity. A very active HER catalyst should possess a low ΔG_{H^*} value close to 0 eV, because a much lower energy ($\Delta G_{H^*} \ll 0$ eV) slows the hydrogen generation process owing to strong H*-binding on the catalyst surface or a sluggish H-releasing step, whereas a too high energy ($\Delta G_{H^*} \gg 0$ eV) leads to an endothermic proton- or electron-transfer process.[31,32]

Herein, the ΔG_{H^*} was probed for the catalyts including the pure active metallic components. The structural models of the main catalytic phases are displayed in Figure 4a. As shown in Figure 4b, Pd/C and Pd@Pt alloy display a ΔG_{H^*} value of 0.201 and −0.167 eV, respectively. In comparison with the (111) facets of the metallic counterparts, it can be reaosnably suggested that the Pd@Pt core−shell structure is significant for enahncing the HER activiy by further lowering the ΔG_{H^*} of Pd. Interestingly, the Pd@PtCu alloy system displays an even much lower ΔG_{H^*} value (−0.094 eV), which is almost equivalent to that of Pt(111) (−0.092 eV) and signifcantly closer to the optimal value of zero than the (111) facet of Pd (−0.198 eV) and Cu (0.223 eV). This demonstrates that the adsorbed H*

DOI: 10.1021/acsenergylett.8b00330
ACS Energy Lett. 2018, 3, 940−945

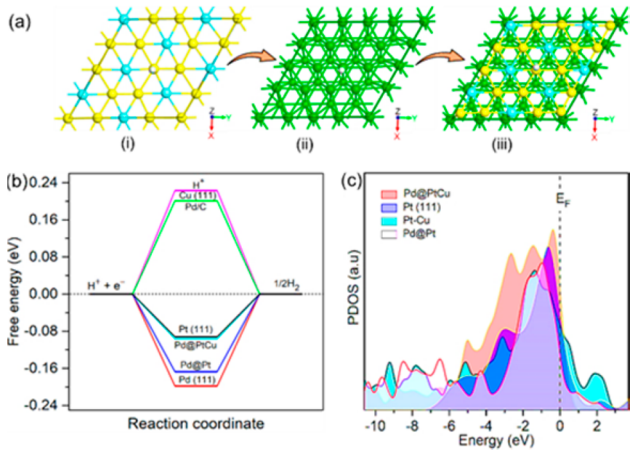

Figure 4. (a) Atomic structural model of catalysts (i) single-layer PtCu, (ii) Pd(111), and (iii) Pd@PtCu. Atoms are Pd (green), Pt (yellow), Cu (aqua), and H (white). (b) Calculated free-energy diagram of catalysts. (c) Projected DOS for atomic hydrogen chemisorbed at the Pt(111), Pt−Cu, Pd@Pt, and Pd@PtCu. The vertical dashed line represents the Fermi level (E_F).

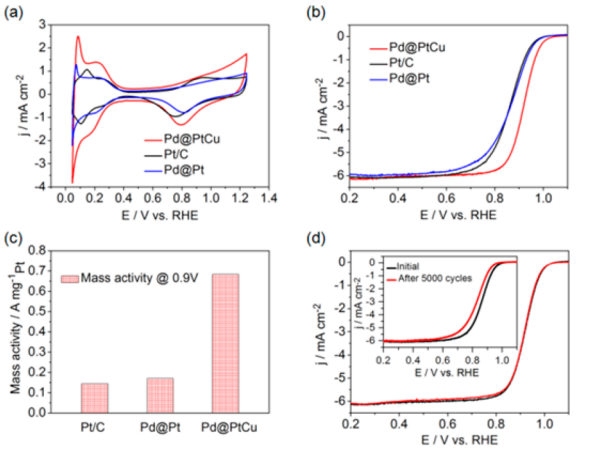

Figure 5. Comparison of electrocatalytic properties of Pd@PtCu/C, Pd@Pt/C, and Pt/C catalysts. (a) CV curves recorded at room temperature in a N_2-purged 0.1 M $HClO_4$ solution at a sweep rate of 50 mV/s. The currents were normalized to the geometric area of the glassy carbon electrode (0.196 cm^2). (b) ORR polarization curves recorded in an O_2-saturated 0.1 M $HClO_4$ solution at 1600 rpm and a sweep rate of 10 mV/s. (c) Mass activity of catalysts normalized to the mass of Pt at 0.9 V versus RHE. (d) ORR polarization curves of Pd@PtCu/C and commercial Pt/C (inset) before and after 5000 cycles.

binds neither too weakly nor strongly to Pd@PtCu, which is favorable for promoting high HER activity. The relatively high ΔG_{H^*} value of Cu(111) and Pd/C indicates unfavorable H*-adsorption, while the lower energy of Pd is due to strong H*-binding compared to the Pt sites. This demonstrates that Pt is the main active site for boosting the HER activity of Pd@PtCu. The DFT analysis is consistent with the experimental results, and both clearly suggest that the neighboring Cu atoms are significant for boosting the interaction between adsorbed H* and Pt atoms, such that they are selectively attacked as "sacrificial atoms" to the neighboring Pt atoms within the alloy system, thereby allowing for maximum utilization of Pt on the Pt−Cu shell as active site for electrocatalytic HER activity.

Furthermore, we probed the density of states (DOS)-based descriptors to analyze the d-orbital active centers (d-band center) of the constituent phases (Pt(111), Pd@Pt, and Pt−Cu) relative to the composite Pd@PtCu system. As displayed in Figure 4c, the highest peak of active center DOS shifts toward the Fermi level in the order of Pd@PtCu (−0.34 eV), Pt(111) (−0.62 eV), Pd@Pt (−0.96 eV), and Pt−Cu (−1.39 eV). The shift to lower energy for the Pd@PtCu coupling can be attributed to the effect of short-range electronic charge transfer which contributes to the H*−Pt bond formation, whereby the hybridization of the adsorbed H* orbital with the Pt d-orbital induces the lowering of the energy. This results in good accord with previous observations in which DFT calculations predict that the activation barrier for the bond breaking of H* from metal surfaces is the lowest if the d-band center is at the Fermi level.[33] This further indicates that the sluggish H*-releasing step can be improved by the dual metal alloy (Pt−Cu) shell on Pd nanocore system (Pd@PtCu) where the high reactivity of Cu benefits the HER kinetic activity of Pt.

To further demonstrate the suitability of such engineered alloy structures for broader electrochemical applications, the ORR activity and stability were also investigated, as displayed in Figure 5. Figure 5a shows the CV curves, which reveal a more positive shift of the peak potential for oxygen reduction on the catalyst surface of Pd@PtCu/C compared to Pd@Pt/C and Pt/C catalysts in 0.1 M $HClO_4$ solution, indicating that Pd@PtCu/C has a lower chemisorption energy and, therefore, more favorable active sites for ORR. Figure 5b shows the LSV curves in which Pd@PtCu/C also exhibits a substantial positive shift in both the onset potential and the half-wave potential by approximately 52 and 56 mV, respectively, as compared to Pd@Pt/C and Pt/C.

To compare the mass activity of the different catalysts, the kinetic current was normalized to the Pt loading (15 $\mu g\ cm^{-2}$). As shown in Figure 5c, at 0.9 V, Pd@PtCu/C has mass activity of 0.70 A mg_{Pt}^{-1}, which is ∼5 times greater than that of Pt/C (∼0.14 A mg_{Pt}^{-1}) and ∼4.1 times greater than that of Pd@Pt/C (∼0.17 A mg_{Pt}^{-1}). At the same time, as shown in Figure 5d, Pd@PtCu/C owns a high durability. After 5000 cycles, it shows only ∼2.0 mV degradation in half-wave potential and about 4.8% decline in mass activity, while a significant loss of ∼32 mV in half-wave potential and ∼56% decline in mass activity for Pt/C (inset of Figure 5d). In addition, from the TEM images of Pd@PtCu/C and Pt/C, taken before and after the ADT (Figure S7), we can see that the Pd@PtCu nanocrystals still maintain the dodecahedral shape without any obvious particle aggregation (Figure S7a,b). In contrast, Pt/C shows severe aggregation and particle growth after the ADT (Figure S7c,d). The enhanced ORR catalytic performance of Pd@PtCu/C catalyst can be attributed to three main factors: (i) Interfacial interactions between the "PtCu shell" and Pd core leads to modification of the electronic structures and the d-band center of the Pt atoms.[34] (ii) The alloying of Pt with Cu efficiently facilitates dissociative adsorption of oxygen, which further increases the amount of Pt active sites.[35] (iii) There are dense twin defects at the surface of Pd@PtCu and more ORR-favorable Pt {111} facets based on the dodecahedral structure, which can boost the catalytic performance.[12] Furthermore, Pd@PtCu has high Pt utilization and activity that benefit from alloying with reactive Cu. Thus, the Cu readily erodes in solution and exposes more Pt sites for kinetic activity, as well as acts as sacrificial catalytic components to prolong the electrochemical activity and durability of the composite catalyst. However, Pt/C lacks the capacity to endure structural stability

DOI: 10.1021/acsenergylett.8b00330
ACS Energy Lett. 2018, 3, 940−945

owing to degradation-induced Pt particle detachment, migration, and aggregation, which drastically reduce the catalytic activity of Pt/C.

In conclusion, we have successfully synthesized new Pd@PtCu nanocrystals with unique core@alloy-shell structure. Owing to the interfacial interactions between the "PtCu alloy shell" and the Pd core, the synergistic effect between Pt and Cu atoms, and the dense twin defects at the surface, such a dodecahedral Pd@PtCu catalyst shows ultrahigh activity and stability for both HER and ORR over Pd@Pt core−shell and commercial Pt/C catalysts. Both the experimental and DFT analyses suggest that Pt is the primary active site. Such high Pt active sites and utilization benefit from alloying with reactive Cu, which readily erodes in solution and exposes more Pt sites for kinetic activity, as well as acts as sacrificial catalytic components to prolong the electrochemical activity and durability of the composite catalyst. This work offers a very attractive strategy for designing highly active electrocatalysts and opens exciting avenues to explore new modulators for designing high-performance-oriented electrocatalytic materials for wider application in electrochemical energy devices.

■ ASSOCIATED CONTENT

Supporting Information

The Supporting Information is available free of charge on the ACS Publications website at DOI: 10.1021/acsenergylett.8b00330.

Experimental section, materials characterization, electrochemical methods, DFT details, TEM images, EDS mapping and line scans, XPS spectra, and additional electrochemical characterizations (PDF)

■ AUTHOR INFORMATION

Corresponding Authors

*E-mail: hedaping@whut.edu.cn.
*E-mail: yuli.xiong@yahoo.com.
*E-mail: msc@whut.edu.cn.

ORCID

Ibrahim Saana Amiinu: 0000-0003-4426-7893
Daping He: 0000-0002-0284-4990
Shichun Mu: 0000-0003-3902-0976

Author Contributions

⊥M.B. and I.S.A. contributed equally to this work.

Notes

The authors declare no competing financial interest.

■ ACKNOWLEDGMENTS

This work was supported by the National Natural Science Foundation of China (51372186, 51672204, and 51701146). We also acknowledge the Center for Materials Research and Analysis of Wuhan University of Technology for TEM (Dr. Zhao Deng) and picture suggestion.

■ REFERENCES

(1) Wang, Y. J.; Wilkinson, D. P.; Zhang, J. Noncarbon support materials for polymer electrolyte membrane fuel cell electrocatalysts. *Chem. Rev.* **2011**, *111*, 7625−7651.

(2) Sha, Y.; Yu, T. H.; Liu, Y.; Merinov, B. V.; Goddard, W. A., III Theoretical Study of Solvent Effects on the Platinum-Catalyzed Oxygen Reduction Reaction. *J. Phys. Chem. Lett.* **2010**, *1*, 856−861.

(3) Cheng, N.; Stambula, S.; Wang, D.; Banis, M. N.; Liu, J.; Riese, A.; Xiao, B.; Li, R.; Sham, T. K.; Liu, L. M.; et al. Platinum single-atom and cluster catalysis of the hydrogen evolution reaction. *Nat. Commun.* **2016**, *7*, 13638.

(4) Dai, L.; Mo, S. G.; Qin, Q.; Zhao, X. J.; Zheng, N. F. Carbon Monoxide-Assisted Synthesis of Ultrathin $PtCu_3$ Alloy Wavy Nanowires and Their Enhanced Electrocatalysis. *Small* **2016**, *12*, 1572−1577.

(5) He, D.; Zhang, L.; He, D.; Zhou, G.; Lin, Y.; Deng, Z.; Hong, X.; Wu, Y.; Chen, C.; Li, Y. Amorphous nickel boride membrane on a platinum-nickel alloy surface for enhanced oxygen reduction reaction. *Nat. Commun.* **2016**, *7*, 12362.

(6) Escudero-Escribano, M.; Malacrida, P.; Hansen, M. H.; Vej-Hansen, U. G.; Velázquez-Palenzuela, A.; Tripkovic, V.; Schiøtz, J.; Rossmeisl, J.; Stephens, I. E. L.; Chorkendorff, I. Tuning the activity of Pt alloy electrocatalysts by means of the lanthanide contraction. *Science* **2016**, *352*, 73−76.

(7) Adzic, R. R.; Zhang, J.; Sasaki, K.; Vukmirovic, M. B.; Shao, M.; Wang, J. X.; Nilekar, A. U.; Mavrikakis, M.; Valerio, J. A.; Uribe, F. Platinum Monolayer Fuel Cell Electrocatalysts. *Top. Catal.* **2007**, *46*, 249−262.

(8) Nilekar, A. U.; Mavrikakis, M. Improved oxygen reduction reactivity of platinum monolayers on transition metal surfaces. *Surf. Sci.* **2008**, *602*, L89−L94.

(9) Kitchin, J. R.; Norskov, J. K.; Barteau, M. A.; Chen, J. G. Modification of the surface electronic and chemical properties of Pt(111) by subsurface 3d transition metals. *J. Chem. Phys.* **2004**, *120*, 10240−10246.

(10) Asano, M.; Kawamura, R.; Sasakawa, R.; Todoroki, N.; Wadayama, T. Oxygen Reduction Reaction Activity for Strain-Controlled Pt-Based Model Alloy Catalysts: Surface Strains and Direct Electronic Effects Induced by Alloying Elements. *ACS Catal.* **2016**, *6*, 5285−5289.

(11) Hwang, D. Y.; Choi, K. H.; Park, J. E.; Suh, D. H. Highly efficient hydrogen evolution reaction by strain and phase engineering in composites of Pt and MoS_2 nano-scrolls. *Phys. Chem. Chem. Phys.* **2017**, *19*, 18356−18365.

(12) He, D. S.; He, D.; Wang, J.; Lin, Y.; Yin, P.; Hong, X.; Wu, Y.; Li, Y. Ultrathin Icosahedral Pt-Enriched Nanocage with Excellent Oxygen Reduction Reaction Activity. *J. Am. Chem. Soc.* **2016**, *138*, 1494−1497.

(13) Bai, S.; Wang, C.; Deng, M.; Gong, M.; Bai, Y.; Jiang, J.; Xiong, Y. Surface Polarization Matters: Enhancing the Hydrogen-Evolution Reaction by Shrinking Pt Shells in Pt-Pd-Graphene Stack Structures. *Angew. Chem., Int. Ed.* **2014**, *53*, 12120−12124.

(14) Han, L.; Liu, H.; Cui, P.; Peng, Z.; Zhang, S.; Yang, J. Alloy Cu_3Pt nanoframes through the structure evolution in Cu-Pt nanoparticles with a core-shell construction. *Sci. Rep.* **2015**, *4*, 6414.

(15) Ren, F.; Lu, H.; Liu, H.; Wang, Z.; Wu, Y.; Li, Y. Surface ligand-mediated isolated growth of Pt on Pd nanocubes for enhanced hydrogen evolution activity. *J. Mater. Chem. A* **2015**, *3*, 23660−23663.

(16) Chen, C.; Kang, Y.; Huo, Z.; Zhu, Z.; Huang, W.; Xin, H. L.; Snyder, J. D.; Li, D.; Herron, J. A.; Mavrikakis, M.; et al. Highly Crystalline Multimetallic Nanoframes with Three-Dimensional Electrocatalytic Surfaces. *Science* **2014**, *343*, 1339−1343.

(17) Bu, L.; Guo, S.; Zhang, X.; Shen, X.; Su, D.; Lu, G.; Zhu, X.; Yao, J.; Guo, J.; Huang, X. Surface engineering of hierarchical platinum-cobalt nanowires for efficient electrocatalysis. *Nat. Commun.* **2016**, *7*, 11850.

(18) Cao, X.; Han, Y.; Gao, C.; Xu, Y.; Huang, X.; Willander, M.; Wang, N. Highly catalytic active PtNiCu nanochains for hydrogen evolution reaction. *Nano Energy* **2014**, *9*, 301−308.

(19) Di Noto, V.; Negro, E. Pt-Fe and Pt-Ni Carbon Nitride-Based 'Core−Shell' ORR Electrocatalysts for Polymer Electrolyte Membrane Fuel Cells. *Fuel Cells* **2010**, *10*, 234−244.

(20) Borbóngonzález, D. J.; Fortunelli, A.; Barcaro, G.; Sementa, L.; Johnston, R. L.; Posada-Amarillas, A. Global Minimum $Pt_{13}M_{20}$ (M = Ag, Au, Cu, Pd) Dodecahedral Core-Shell Clusters. *J. Phys. Chem. A* **2013**, *117*, 14261−14266.

DOI: 10.1021/acsenergylett.8b00330
ACS Energy Lett. 2018, 3, 940−945

(21) Nosheen, F.; Zhang, Z. C.; Zhuang, J.; Wang, X. One-pot fabrication of single-crystalline octahedral Pt-Cu nanoframes and their enhanced electrocatalytic activity. *Nanoscale* **2013**, *5*, 3660−3663.
(22) Han, L.; Cui, P.; He, H.; Liu, H.; Peng, Z.; Yang, J. A seed-mediated approach to the morphology-controlled synthesis of bimetallic copper-platinum alloy nanoparticles with enhanced electrocatalytic performance for the methanol oxidation reaction. *J. Power Sources* **2015**, *286*, 488−494.
(23) Ye, W.; Chen, S.; Ye, M.; Ren, C.; Ma, J.; Long, R.; Wang, C.; Yang, J.; Song, L.; Xiong, Y. $Pt_4PdCu_{0.4}$ alloy nanoframes as highly efficient and robust bifunctional electrocatalysts for oxygen reduction reaction and formic acid oxidation. *Nano Energy* **2017**, *39*, 532−538.
(24) Jia, Y.; Cao, Z.; Chen, Q.; Jiang, Y.; Xie, Z.; Zheng, L. Synthesis of composition-tunable octahedral Pt−Cu alloy nanocrystals by controlling reduction kinetics of metal precursors. *Sci. Bull.* **2015**, *60*, 1002−1008.
(25) Yin, Y.; Rioux, R. M.; Erdonmez, C. K.; Hughes, S.; Somorjai, G. A.; Alivisatos, A. P. Formation of Hollow Nanocrystals Through the Nanoscale Kirkendall Effect. *Science* **2004**, *304*, 711−714.
(26) Crist, B. V. BE lookup table for signals from elements and common chemical species. In *Handbook of Monochromatic XPS Spectra: The Elements of Native Oxides*; Wiley: Chichester, U.K., 1999.
(27) Stadnichenko, A. I.; Sorokin, A. M.; Boronin, A. I. XPS, UPS, and STM studies of nanostructured CuO films. *J. Struct. Chem.* **2008**, *49*, 341−347.
(28) Cao, Z.; Chen, Q.; Zhang, J.; Li, H.; Jiang, Y.; Shen, S.; Fu, G.; Lu, B.; Xie, Z.; Zheng, L. Platinum-nickel alloy excavated nano-multipods with hexagonal close-packed structure and superior activity towards hydrogen evolution reaction. *Nat. Commun.* **2017**, *8*, 15131.
(29) Weng, X.; Liu, Q.; Wang, A. J.; Yuan, J.; Feng, J. J. Simple one-pot synthesis of solid-core@porous-shell alloyed PtAg nanocrystals for the superior catalytic activity toward hydrogen evolution and glycerol oxidation. *J. Colloid Interface Sci.* **2017**, *494*, 15−21.
(30) Ying, J.; Jiang, G.; Cano, Z. P.; Han, L.; Yang, X. Y.; Chen, Z. Nitrogen-doped hollow porous carbon polyhedrons embedded with highly dispersed Pt nanoparticles as a highly efficient and stable hydrogen evolution electrocatalyst. *Nano Energy* **2017**, *40*, 88−94.
(31) Noerskov, J. K.; Bligaard, T.; Logadottir, A.; Kitchin, J. R.; Chen, J. G.; Pandelov, S.; Stimming, U. Trends in the Exchange Current for Hydrogen Evolution. *J. Electrochem. Soc.* **2005**, *152*, J23−J26.
(32) Duan, H.; Li, D.; Tang, Y.; He, Y.; Ji, S.; Wang, R.; Lv, H.; Lopes, P. P.; Paulikas, A. P.; Li, H.; et al. High-Performance Rh_2P Electrocatalyst for Efficient Water Splitting. *J. Am. Chem. Soc.* **2017**, *139*, 5494−5502.
(33) Santos, E.; Schmickler, W. d-Band Catalysis in Electrochemistry. *ChemPhysChem* **2006**, *7*, 2282−2285.
(34) Mazumder, V.; Chi, M.; More, K. L.; Sun, S. Core/Shell Pd/FePt Nanoparticles as an Active and Durable Catalyst for the Oxygen Reduction Reaction. *J. Am. Chem. Soc.* **2010**, *132*, 7848−7849.
(35) Dhavale, V. M.; Kurungot, S. Cu-Pt Nanocage with 3-D Electrocatalytic Surface as an Efficient Oxygen Reduction Electrocatalyst for a Primary Zn-Air Battery. *ACS Catal.* **2015**, *5*, 1445−1452.

DOI: 10.1021/acsenergylett.8b00330
ACS Energy Lett. 2018, 3, 940−945